Changes in Thermodynamic Stability of von Willebrand Factor Differentially Affect the Force-Dependent Binding to Platelet GPIbα

Matthew Auton,[†‡‡] Erik Sedlák,[‡] Jozef Marek,[§] Tao Wu,[¶] Cheng Zhu,[¶‖] and Miguel A. Cruz[‡‡*]
[†]Department of Bioengineering, and [‡]Department of Biochemistry and Cell Biology, Rice University, Houston, Texas; [§]Department of Biophysics, Institute of Experimental Physics, Slovak Academy of Sciences, Košice, Slovakia; [¶]Woodruff School of Mechanical Engineering, and [‖]Coulter Department of Biomedical Engineering, Georgia Institute of Technology, Atlanta, Georgia; and [‡‡]Thrombosis Research Section, Baylor College of Medicine, Houston, Texas

ABSTRACT In circulation, plasma glycoprotein von Willebrand Factor plays an important role in hemostasis and in pathological thrombosis under hydrodynamic forces. Mutations in the A1 domain of von Willebrand factor cause the hereditary types 2B and 2M von Willebrand disease that either enhance (2B) or inhibit (2M) the interaction of von Willebrand factor with the platelet receptor glycoprotein Ibα. To understand how type 2B and 2M mutations cause clinically opposite phenotypes, we use a combination of protein unfolding thermodynamics and atomic force microscopy to assess the effects of two type 2B mutations (R1306Q and I1309V) and a type 2M mutation (G1324S) on the conformational stability of the A1 domain and the single bond dissociation kinetics of the A1-GPIbα interaction. At physiological temperature, the type 2B mutations destabilize the structure of the A1 domain and shift the A1-GPIbα catch to slip bonding to lower forces. Conversely, the type 2M mutation stabilizes the structure of the A1 domain and shifts the A1-GPIbα catch to slip bonding to higher forces. As a function of increasing A1 domain stability, the bond lifetime at low force decreases and the critical force required for maximal bond lifetime increases. Our results are able to distinguish the clinical phenotypes of these naturally occurring mutations from a thermodynamic and biophysical perspective that provides a quantitative description of the allosteric coupling of A1 conformational stability with the force dependent catch to slip bonding between A1 and GPIbα.

INTRODUCTION

Originally described by Erik von Willebrand in 1926, von Willebrand disease (VWD) is the most common hereditary bleeding disorder in humans (1). The inheritance of VWD is autosomal dominant, affecting both sexes, and results from a quantitative deficiency (types 1 and 3) and/or a qualitative abnormality (type 2) of the von Willebrand factor (VWF) protein, whose primary role in hemostasis is to initiate the adherence of platelets to the subendothelium at sites of vascular injury (2,3).

VWF is a multidomain glycoprotein that is secreted into the blood as a large multimeric polymer from vascular endothelial cells. Mature VWF consists of a 2050-residue subunit that contains multiple copies of A, B, C, and D type domains that are arranged in the order D-D3-A1-A2-A3-D4-B1-B2-B3-C1-C2-CK (cystine knot) (4–6). Under the influences of blood flow, the interaction between VWF and platelets is mediated by the A1 domain which binds the platelet glycoprotein Ibα (GPIbα), contributing to the arrest of bleeding as well as to the pathologic occlusion of diseased vessels under elevated shear stress (7–10).

Two subtypes of type 2 VWD are characterized by either enhanced (type 2B) or deficient (type 2M) platelet-VWF interactions due to point mutations located specifically in the A1 domain of VWF (11,12). Clinically, type 2B patients are hyperresponsive to ristocetin-induced platelet agglutination due to the abnormally high affinity of VWF for platelet GPIbα. In addition, higher molecular weight multimers of VWF are absent, presumably because the enhanced VWF interaction with platelets increases its susceptibility to proteolysis by the enzyme, ADAMTS13. Conversely, type 2M patients are typically insensitive to ristocetin-induced platelet agglutination due to a low VWF affinity for platelet GPIbα and the multimerization of VWF is normal (3). These contrary effects of type 2B and type 2M mutations on VWF function emphasize the critical role of the A1 domain interaction with GPIbα in primary hemostasis. However, the structural basis by which these mutations cause clinically opposite phenotypes is not understood.

We have applied equilibrium thermodynamics of protein unfolding and kinetics of single-bond dissociation to elucidate how two common type 2B mutations (R1306Q and I1309V) and a type 2M mutation (G1324S) affect the intrinsic conformational stability of A1 and the bond stability of the GPIbα interaction with A1. Fig. 1 illustrates the structural locations of these clinical mutations in the A1 domain. We have performed urea denaturation of A1 as a function of temperature, with thermal denaturation of A1 by differential scanning calorimetry and atomic force microscopy to assess structural stability and the bond strength of the A1-GPIbα interaction.

Submitted March 10, 2009, and accepted for publication May 1, 2009.

*Correspondence: miguelc@bcm.tmc.edu

Matthew Auton performed the isothermal denaturation studies and phase diagram analysis, Erik Sedlák performed the DSC measurements, Jozef Marek provided the software and analysis of the DSC results, and Tao Wu performed the AFM measurements of single-bond lifetimes. All authors contributed to the writing of this article.

Erik Sedlák's present address is Department of Biochemistry, University of Texas Health Science Center-San Antonio, San Antonio, Texas.

Editor: Josh Wand.

0006-3495/09/07/0618/10 $2.00

doi: 10.1016/j.bpj.2009.05.009

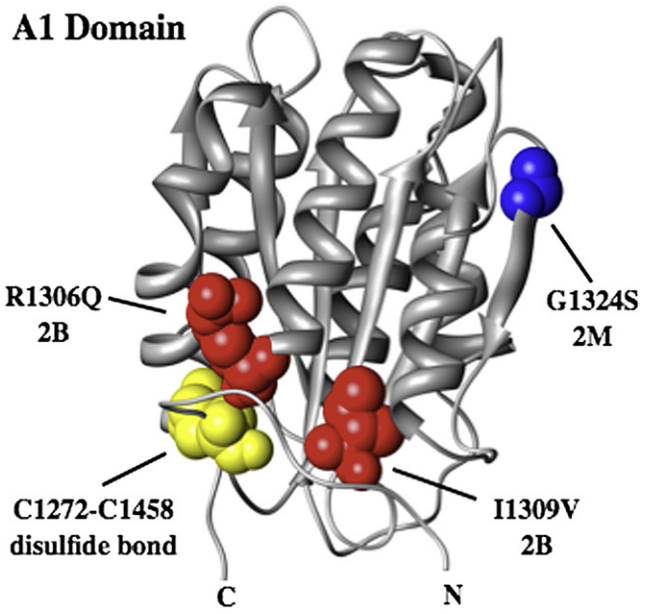

FIGURE 1 Structure of the A1 domain with the type 2B, R1306Q and I1309V, mutations indicated in red and the type 2M mutation, G1324S, in blue. The disulfide bond is yellow. The structure was drawn using Chimera (http://www.cgl.ucsf.edu/chimera/).

Previously, we have shown that urea unfolds the native conformation of the A1 domain to an intermediate that has significant secondary structure (13). Here we show that the native conformation of A1 is destabilized by the type 2B mutations and is stabilized by the type 2M mutation at physiological temperature. We have also demonstrated previously that the A1 domain forms catch bonds with GPIbα, a property that regulates platelet-rolling velocities on VWF as flow increases (14). Here we show that both of the type 2B mutations enhance bond lifetimes at low force, resulting in a left-shift of the catch bond toward low force for I1309V and a loss of a catch bond for R1306Q. In contrast, the type 2M G1324S mutation decreases the bond lifetime at low force and right-shifts the catch bond toward higher forces than observed for wild-type (WT) A1. These correlative observations demonstrate the mutual relationship between the conformational stability of VWF and its capacity to bind platelets at physiological tethering forces. These observations also unite equilibrium thermodynamics of protein stability with force-dependent catch to slip-bond transitions that occur in proteins involved in cellular adhesion. Our results suggest a fundamental mechanism by which the intrinsic stability of the A1 domain regulates the binding to GPIbα, and provide the first experimental evidence for conformational allostery in the interaction between the VWF A1 domain and platelet GPIbα.

METHODS

Recombinant WT, R1306Q, I1309V, and G1324S VWF-A1 domain variants were produced as previously described (15,8). Glycocalicin (the extracellular fragment of GPIbα) was purified from outdated human platelet-rich plasma obtained from the Saint Luke's Hospital Transfusion Services as previously described (16).

All isothermal denaturations of the WT A1 domain and type 2 VWD mutants were performed in 10 mM NaAcetate, 10 mM Phosphate, 10 mM Glycine, 150 mM NaCl, 2 mM ethylenediaminetetraacetic acid (EDTA), pH = 8 buffer at a protein concentration of 10 μM. The solutions of protein at each concentration of urea or guanidinium hydrochloride (GdmHCl) were allowed to equilibrate at 5°C and 15°C overnight and at 25°C and 35°C for 4–6 h. Circular dichroism was used to monitor the unfolding as previously described (13).

Differential scanning calorimetry (DSC) measurements were performed on a VP-DSC instrument (MicroCal, GE Healthcare, Piscataway, NJ) at 2 atm after general guidelines for calorimetry (17). In all cases, 0.5 mg/ml of protein, was solubilized in 10 mM NaAcetate, 10 mM Phosphate, 10 mM Glycine, 150 mM NaCl, 2 mM EDTA at pH = 8.0. Thermal transitions were calorimetrically irreversible due to protein aggregation at high temperature. All DSC traces were corrected for an irreversible scan that was used as the baseline.

A detailed description of the thermodynamic phase diagram analysis of the isothermal urea denaturations and the differential scanning calorimetry analysis is provided in the Supporting Material along with the corresponding data tables.

The atomic-force microscopy (AFM) force-clamp single-bond lifetime measurement method has been described (14) using our custom-made AFM (design adapted from V. Moy, University of Miami). Commercial cantilevers (TM Microscopes, Sunnyvale, CA) with spring constants from 4 to 13 pN nm^{-1} were calibrated by the thermal fluctuation method (18). Briefly, 15 μL of WT or mutant A1 (10 μg/mL) was incubated on each of two spots on a petri dish overnight at 4°C. To reduce nonspecific binding, a polystyrene petri dish was prewashed with absolute ethanol and dried with argon gas at 4°C overnight. The petri dish was washed three times with phosphate-buffered saline (PBS) and blocked with PBS containing 1% bovine serum albumin. AFM cantilevers were soaked in PBS containing 1% bovine serum albumin (for negative control) or 10 μg/mL glycocalicin at 4°C overnight. Lifetimes of GPIbα/A1 bonds were measured in repeated test cycles consisting of the following steps:

Step 1. Move the AFM tip to touch the Petri dish for 0.02 s.
Step 2. Retract it ~4 nm above the surface.
Step 3. Hold it for 1 s to allow for bond formation.
Step 4. Further retract it a predetermined distance, to see whether binding occurs.
Step 5. If binding occurs, ramp to the preset force to determine whether the bond survives.
Step 6. If the bond survives, measure the length of time until the bond breaks (i.e., lifetime of the bond) at that force.
Step 7. Retract the AFM tip to the starting position.

Adhesion frequencies were <20%. Approximately twenty-percent of adhesions yielded measurable lifetimes. Lifetime histograms were representative of those published in the literature (19,20). Each lifetime-versus-force curve includes several hundreds of measurements (several tens of lifetime measurements per force bin).

RESULTS

In the following, we first describe the denaturant and temperature-dependent conformational stability of the A1 domain containing the type 2B (R1306Q and I1309V) and 2M (G1324S) mutations using the linear extrapolation and phase diagram methods for isothermal urea-induced unfolding and simplified Lumry-Eyring methods for the thermal unfolding. After that, we proceed to the effects of these mutations on the force-dependent-catch-to-slip-bond transitions in the A1-GPIbα interaction and demonstrate the relationship between these two intrinsic properties of the A1 domain.

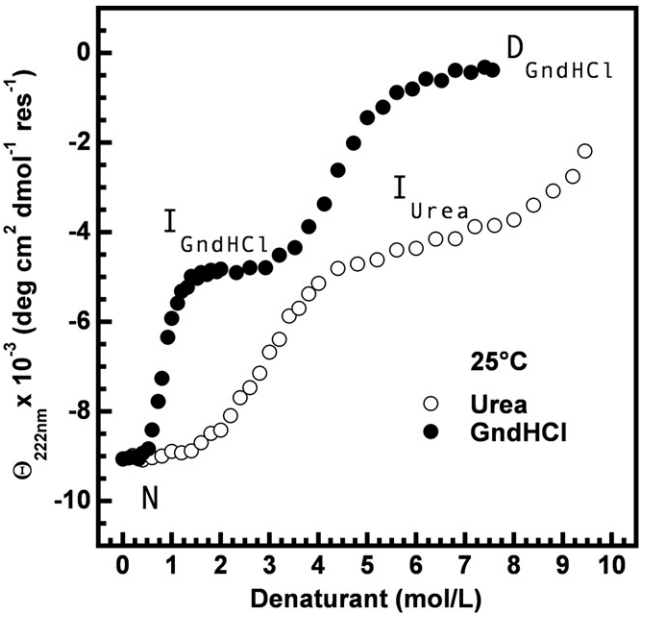

FIGURE 2 Urea and Guanidine HCl (GndHCl) denaturation of wild-type VWF A1 domain at 25°C monitored by circular dichroism at 222 nm to illustrate the three-state character of the unfolding. Open symbols represent the urea data and solid symbols represent the GndHCl data.

Urea and guanidine HCl-induced three-state reversible unfolding of the A1 domain

Previously, we reported that the A1 domain unfolds in a three-state manner through a well-defined intermediate structure that does not fully denature in urea (13). In Fig. 2, circular dichroism is used to monitor the unfolding as a function of denaturant molarity which shows that guanidine HCl (GndHCl), a much stronger denaturant, is able to fully resolve the second transition. Comparison of the urea and GndHCl isothermal denaturations at 25°C of WT A1 shows that the first transition from $N \rightleftharpoons I$ in urea is shifted to lower concentrations of GndHCl. The second transition, $I \rightleftharpoons D$, which is only partially attained in urea, is fully resolved at higher concentrations of GndHCl. It should be noted that the unfolding of A1 induced by both urea and GndHCl is fully reversible. Because of the high salt effects that accompany GndHCl-induced protein denaturation, we used GndHCl only for illustrating the three-state unfolding character of the A1 domain. Hereafter, we use urea and temperature to distinguish the effects of clinical mutations on the structural stability of A1.

The stability profile of the A1 domain assessed by the phase diagram method

In Fig. 3, we report the isothermal urea denaturation of WT A1, the type 2B VWD mutants, R1306Q and I1309V, and the type 2M VWD mutant, G1324S, at 5°C, 15°C, 25°C, and 35°C. The results of Fig. 3 illustrate some important features of the structural transitions.

First, the native state secondary structure content of the type 2 VWD A1 mutants is greater than for WT, as indicated by the increased mean residue molar ellipticity.

Second, the clinical mutations only affect the $N \rightleftharpoons I$ transition and the $I \rightleftharpoons D$ transition is not altered by the mutations. To confirm this, we also denatured these A1 domain mutants with GndHCl at 25°C and found that the $I \rightleftharpoons D$ transitions were identical for all protein mutants (data not shown). At any given temperature, the secondary structure content of the intermediate state is identical for all of the protein mutants. However, the secondary structure content of the intermediate has a strong dependence on urea concentration, and as the temperature is increased, the secondary structure of the intermediate also increases, as is evident from the continual decrease of the intermediate state baseline as a function of temperature. This indicates that the structure of the intermediate is highly variable, resulting in expansion with increasing urea and contraction with increasing temperature.

Third, the type 2M G1324S mutation stabilizes the A1 domain, as is evident by the higher urea concentration (greater $c_{1/2}$) required to unfold the native structure. The type 2B mutants, however, unfold within the same urea concentrations as the WT A1 domain.

Fourth, the cooperativity of the urea unfolding (*m*-value) for all the disease mutants, indicated by the width of the transition, has greater temperature dependence than for the WT A1 domain. The *m*-value distinguishes the thermodynamic stability of type 2B mutants from WT, rather than the $c_{1/2}$ of the unfolding transition.

The phase diagram method illustrates these observations more clearly (21). In Fig. 4, we have plotted all of the thermodynamic parameters obtained from the fitting of the data in Fig. 3 to Eq. S1 in the Supporting Material along with the results of a two-dimensional global fit of the data for all temperatures and urea concentrations, Eq. S2 (*lines*), as a function of temperature. The thermodynamic parameters resulting from the phase diagram analysis are given in Table S1. Fig. 4 shows the intrinsic stability against unfolding in the absence of urea, ΔG^0, the urea-induced unfolding cooperativity, *m*-value, the midpoint of the urea unfolding transition, $c_{1/2}$, and the populations of native (N), intermediate (I), and denatured (D) states as a function of temperature.

We first describe the energetics associated with the first unfolding transition, $N \rightleftharpoons I$. Fig. 4 *A* shows that the native-state stability of A1 containing the type 2M mutation, G1324S (*blue*), is at all temperatures greater than the WT A1. The type 2B mutations (*red*) at low temperatures are slightly more stable than WT A1, but at physiological temperature, these mutations cause A1 to become less stable than WT. This stability trend is also evident by the melting temperature, T_m, at which $\Delta G^0 = 0$. The T_m for G1324S increases and the T_m for both type 2B mutants decreases relative to WT A1 (Fig. 4 *A* and Table S1). Another feature of the stability curves for the $N \rightleftharpoons I$ transition is the increased apparent heat capacity of unfolding (ΔC_p^0) for the type 2

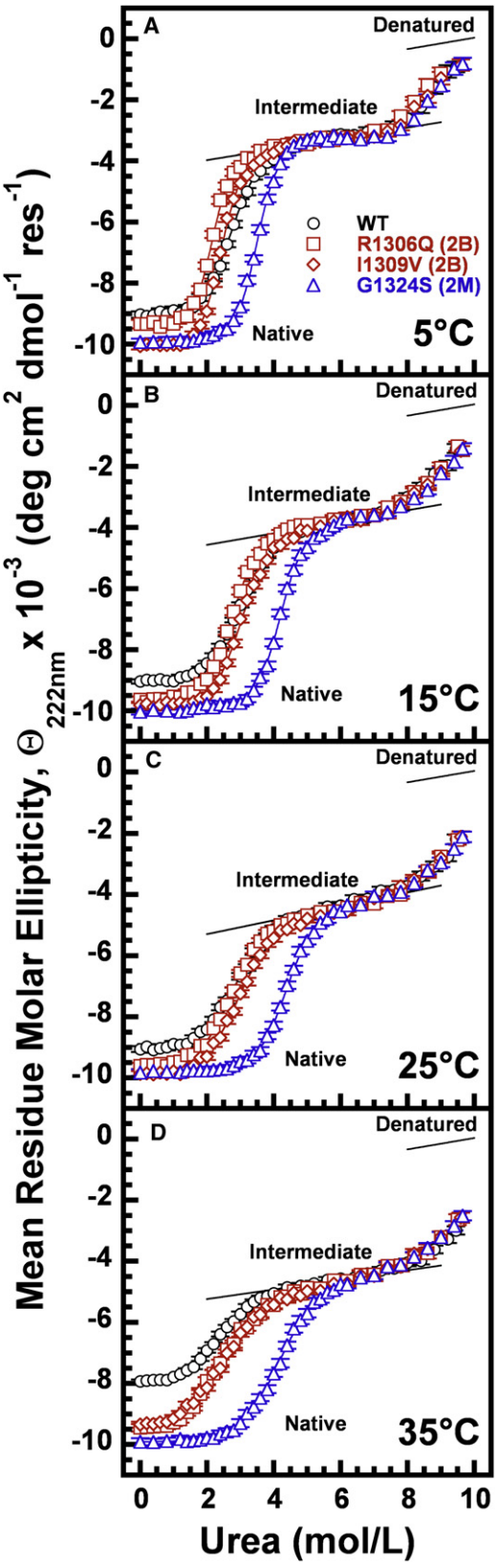

FIGURE 3 Urea denaturation of wild-type VWF A1 domain (*black circles*), the type 2B VWD gain-of-function mutations R1306Q (*red squares*) and I1309V (*red diamonds*), and the type 2M VWD loss-of-function mutation G1324S (*blue triangles*) at 5°C, 15°C, 25°C, and 35°C. Lines represent the results of the fit of the data to Eq. S1.

mutants of A1 relative to WT (Table S1), which results in the increased curvature of the ΔG^0 as a function of temperature. ΔC_p^0 is highly proportional to changes in solvent-accessible surface area upon unfolding and an increase in ΔC_p^0 as a result of the mutation indicates that these mutants result in more extensive unfolding than WT A1 (22–24).

Fig. 4 *B* shows that the temperature dependence of the urea-induced unfolding cooperativity for the mutations is greater than WT, as is evident from the increased slope ($\partial_T m$) of the linear dependence of the *m*-value on temperature. Since the *m*-value is directly representative of the size of the cooperative unit, a greater magnitude of *m* indicates a greater amount of the protein structure participates in the unfolding (22,24,25). At low temperature, where stability is maximal, the size of the unfolding cooperative unit is larger than WT for all clinical mutants. At higher temperatures, the greater temperature dependence of *m* causes the size of the cooperative unit to be comparable to WT for G1324S and to decrease relative to WT for both of the type 2B mutants.

The urea-temperature phase diagram in Fig. 4 *C*, gives the 50% phase separation lines between states. The shape of the curves are essentially thermal stability curves (ΔG^0) that are modified by the temperature-dependent *m*-value and they define the regions on the urea-temperature plane where conformational states of the A1 domain are populated (21). The linear extrapolation model (see the Supporting Material) states that the stability of a protein depends on the $c_{1/2}$ as well as the *m*-value. Although the increased $c_{1/2}$ required to unfold the type 2M G1324S mutant results in its enhanced thermodynamic stability over WT A1, the urea $c_{1/2}$ of the type 2B mutants (R1306L and I1309V) are very similar to WT A1. The decreased stability of the type 2B mutants relative to WT A1 at physiological temperature is a direct consequence of the strongly temperature dependent *m*-values resulting from these VWD mutations.

Finally, Fig. 4 *D* shows the populations of native, intermediate, and denatured states as a function of temperature. At 37°C, the lower stability of the type 2B mutations significantly increases the population of the intermediate conformation. The intermediate is 13% populated for R1306Q and 10% populated for I1309V, whereas, for WT, it is only 3% populated. For G1324S, the population of the intermediate state is negligible at physiological temperature.

For all the A1 mutants studied, the unfolding of the intermediate structure from $I \rightleftharpoons D$ is independent of the mutation. Fig. 2 shows that relative to fully denatured state, this partially folded intermediate has significant secondary structure and the thermodynamic stability of the intermediate is greater than the native state stability (see Fig. 4 *A*, *solid symbols*). Thermodynamically, classical two-state unfolding only occurs if the stability of higher order structures exceeds the stability of lower order structures (23). The three-state

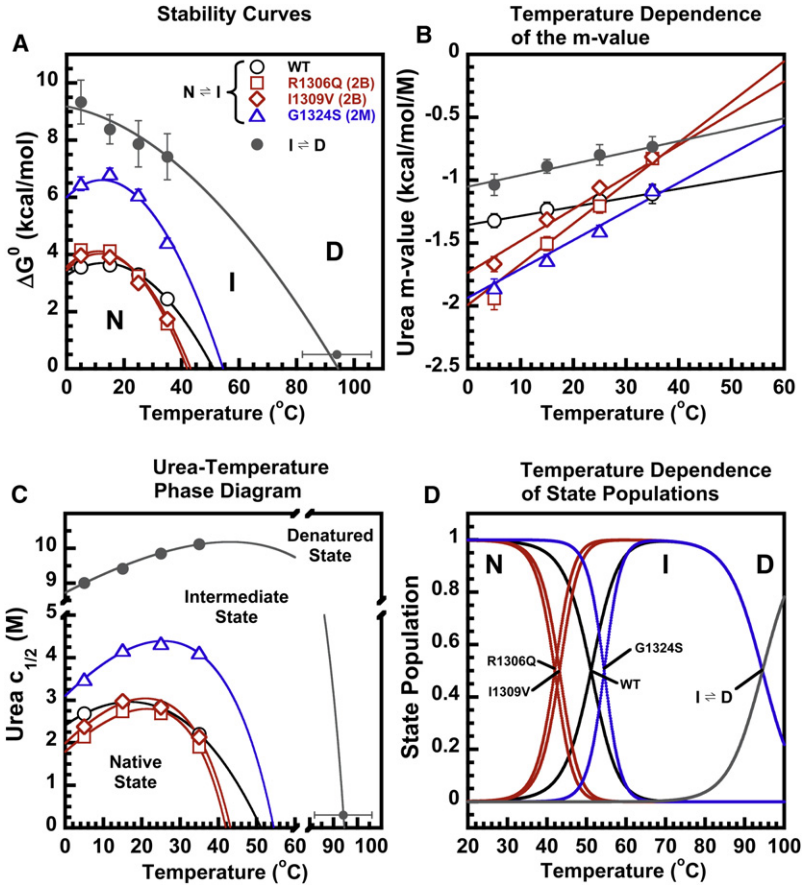

FIGURE 4 Temperature dependence of the thermodynamic parameters derived from the isothermal urea-induced unfolding of the VWF A1 domain shown in Fig. 3. Symbols are identical to Fig. 3. (*A*) Thermodynamic stability (ΔG^0) of the A1 domain in the absence of urea as a function of temperature defines the stability curve. (*B*) Temperature dependence of the urea-induced unfolding cooperativity (*m*-value). (*C*) Urea-temperature phase diagram. Urea $c_{1/2}$ versus temperature represents the 50% phase separation line between the native and intermediate states of A1 and between the intermediate and denatured states of A1. (*D*) Populations of the native, intermediate, and denatured states as a function of temperature. At 37°C, the population of the intermediate for R1306Q is 13%, I1309V is 10%, WT is 3%, and G1324S is <0.1%. The $N \rightleftharpoons I$ transition is represented by open symbols and the $I \rightleftharpoons D$ transition by shaded circles. Data points represent parameters derived from independent fits of the data in Fig. 3 to Eq. S1 and lines represent the results of a global fit of the data in Fig. 2 to Eq. S2.

unfolding character of A1 results from the high stability of the lower order structures making up the intermediate state, which exceeds the native state stability. The thermal stability of the intermediate is also associated with a very low apparent heat capacity (Table S1) and the *m*-value of the intermediate is less than the native state. This indicates that the intermediate state retains a sizeable hydrophobic core that can be forced to unfold in a cooperative manner with high concentrations of denaturants. The intermediate state also has a very high melting temperature $T_m = 94 \pm 12$°C, indicating that the fully denatured state is never populated under physiological conditions (Fig. 4 *D*). All of the aforementioned observations indicate that the intermediate state consists of an ensemble of conformations with different degrees of residual structure. This variable thermodynamic character of the intermediate state, as observed by urea-induced expansion and temperature-induced contraction, is the likely cause of the highly temperature dependent *m*-values that we observe for the $N \rightleftharpoons I$ transition.

Differential scanning calorimetry: irreversible thermal denaturation of the A1 domain in the absence of denaturant

Although the urea denaturation of the A1 domain is reversible, thermal denaturation of the A1 domain is calorimetrically irreversible as no thermal effect is observed in a second heating of the protein solution. A characteristic of thermal irreversibility is the scan rate dependence of the apparent T_{trs} (temperature at the maximum of the heat capacity profile), which decreases with slower scan rates. The effect of the scan rate on the calorimetric profiles indicates that they correspond to irreversible, kinetically controlled transitions, in aqueous solution. Comparing the DSC transitions in Fig. 5 shows a net decrease in the apparent T_{trs} values at all temperature scan rates relative to WT A1 for both type 2B mutants of A1 (R1306Q and I1309V) and an increase in the apparent T_{trs} for the type 2M G1324S mutant of A1 (Table S2). When analyzed by the two-state irreversible model given by Eq. S5 and Eq. S6, the half-life at 37°C, calculated from the temperature dependence of the irreversible rate constant, decreases relative to WT for the type 2B mutants and is substantially increased for the type 2M mutant (Table S2). Both of these observations indicate that the type 2B mutations destabilize the A1 domain and the type 2M mutation stabilizes the A1 domain.

The most general mechanism of irreversible protein unfolding is the Lumry-Eyring model, in which the native conformation reversibly unfolds to an intermediate that is irreversibly converted to a final state, $N \rightleftharpoons I \rightarrow F$ (26). The fitting of the calorimetric data to Eq. S5 indicates that the thermal denaturation of A1 proceeds without significant

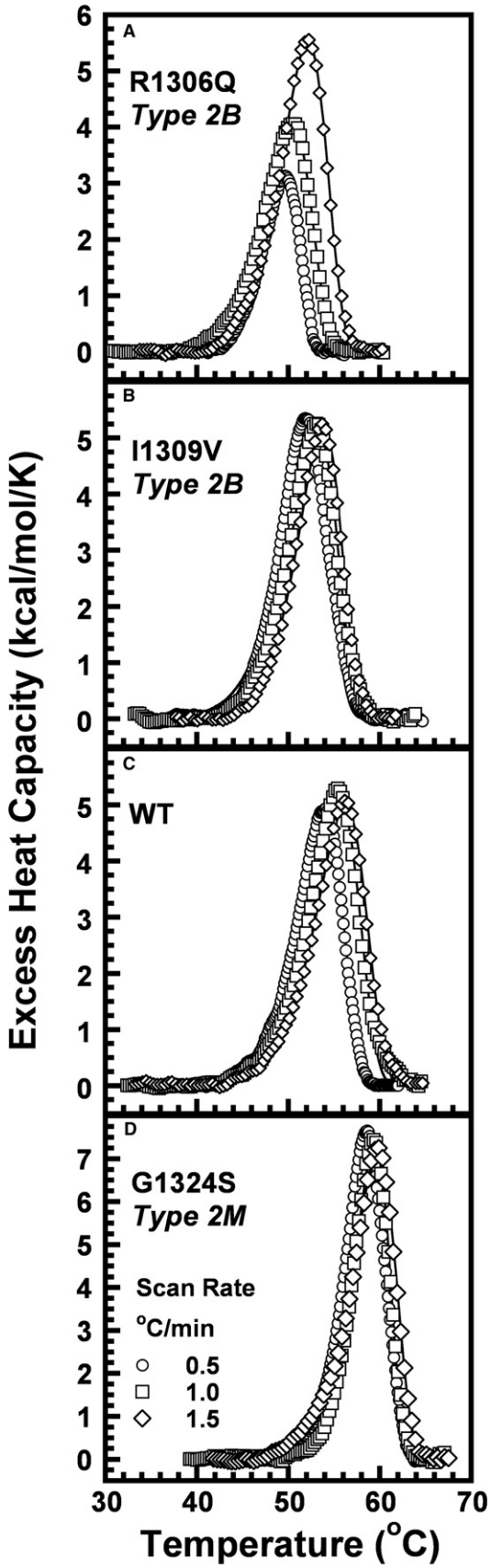

population of the intermediate conformation of the protein (I), $N \rightarrow F$. This limiting model of the thermal denaturation does not mean that the native conformation of A1 undergoes an irreversible alteration. As pointed out by Plaza del Pino et al., the irreversible step is still $I \rightarrow F$ as in the Lumry-Eyring model, but the rate of this step is fast, resulting in a low population of the intermediate in the temperature range of the DSC transition (27). The thermal irreversibility in the absence of urea also does not contradict the conclusions obtained from the reversible isothermal urea denaturation. Lumry and Eyring, in their classical article on protein conformational changes, stated that ''hydrogen bonds between urea molecules and peptide linkages appear to isolate individual unfolded polypeptides to prevent, at least under mild conditions of time and temperature, the polymolecular aggregation which frequently establishes irreversibility in thermal transconformations of secondary structures'' (26). Furthermore, in a more recent article, Rodriguez-Larrea et al. showed that low concentrations of denaturants can restore thermal reversibility (28).

Despite the thermal irreversibility in the absence of urea, both thermodynamic analyses for isothermal urea denaturation and differential scanning calorimetry are in qualitative agreement showing that the type 2B mutants of A1 are destabilized and the type 2M mutant of A1 is stabilized relative to the WT A1 domain. These changes in conformational stability are strongly correlated with the GPIbα binding properties of the A1 domain, as described in the next section.

AFM force-clamp single-bond lifetime measurements

The results obtained from AFM experiments are an extension of our previous work, where we analyzed WT A1 and the R1306Q mutation (14). Fig. 6 shows the force-dependent lifetimes of single bonds of the interaction between the A1 domain and glycocalicin, the extracellular fragment of the platelet GPIbα surface receptor. Here, the bond lifetime of the A1-glycocalicin interaction was measured as a function of the applied force. In the case of the WT A1 domain, the lifetimes of the interaction with glycocalicin exhibited a biphasic character representative of a transition from catch bonds at low force to slip bonds at higher force (Fig. 6). At low bond force, increasing the force enhanced the bond lifetime (catch bond) until an optimal force was attained where the bond lifetime was maximal (~20 pN). Further increases in bond force resulted in decreased bond lifetimes (slip bonds). The type 2M G1324S mutation shifted the catch-bond character of the A1 domain to a higher bond force required for maximal bond lifetime (~40 pN). The type 2B

FIGURE 5 DSC scans of the VWF A1 domain type 2B VWD gain-of-function mutations R1306Q and I1309V (*A* and *B*), wild-type A1 (*C*), and the type 2M VWD loss-of-function mutation G1324S (*D*) at scan rates 0.5 K/min (*circles*), 1.0 K/min (*squares*), and 1.5 K/min (*diamonds*). Lines represent the results of the fit of the data to Eq. S5.

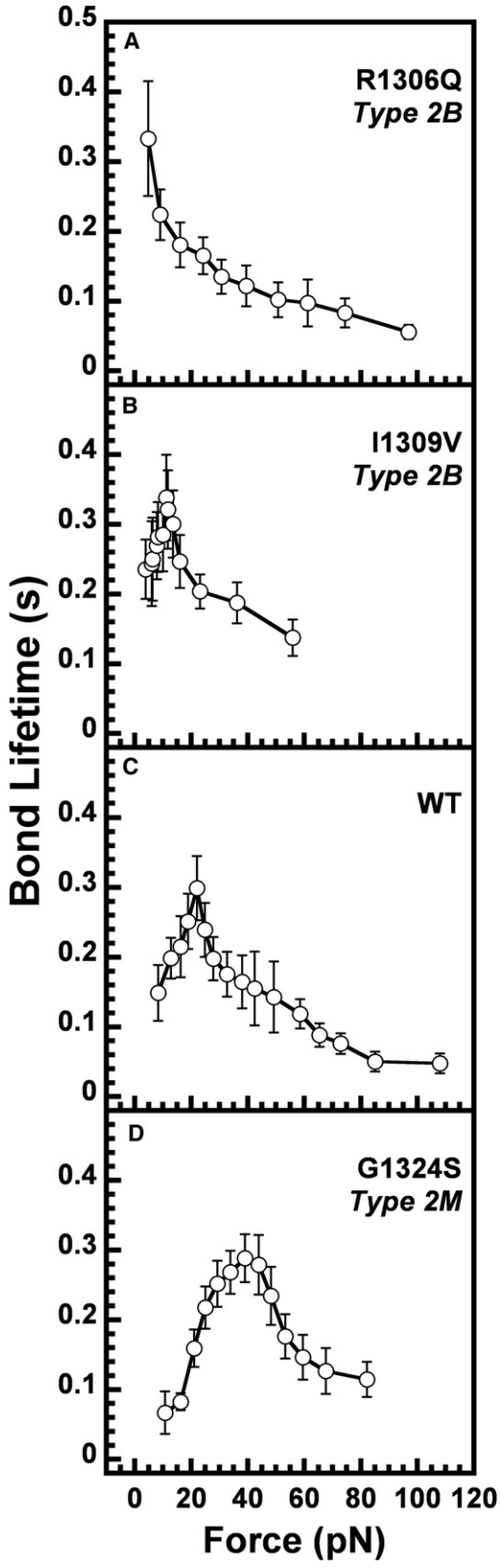

FIGURE 6 A1-GPIbα bond lifetime versus bond force for the type 2B VWD gain-of-function mutations R1306Q and I1309V (*A* and *B*), the WT A1 domain (*C*), and the type 2M VWD loss-of-function mutation G1324S (*D*). The data in panels *A* and *C* were obtained from Yago et al. (14). The data are presented as the mean ± the standard error of the mean.

mutation I1309V decreased the force required for the catch bond (~11 pN) and R1306Q abolished the catch bonds, forming only slip bonds with maximal bond lifetimes at the lowest applied force (<5 pN). These shifts in catch to slip bonding between A1 and GPIbα also change the bond lifetime at low force. The bond lifetime at low force for the type 2B mutations is enhanced relative to WT A1 and diminished for the type 2M mutation.

Rank orders and correlations between the mutational effects on intrinsic stability of A1 and its capacity to bind GPIbα

We have determined the effects of VWD type 2B and type 2M mutations on two fundamental properties of the A1 domain: the intrinsic thermodynamic stability of A1; and the kinetics of the bond dissociation between A1 and GPIbα. From a thermodynamic point of view, we find that both type 2B mutations destabilize the A1 domain and the type 2M mutation stabilizes the A1 domain. The rank order of the mutational effects on conformational stability as given by $\Delta G^0_{37^\circ C,N\rightleftharpoons I}$ and $T_{m,N\rightleftharpoons I}$ (Table S1) determined from the phase diagram method and T_{trs}, T^* and the half-life ($\tau_{37^\circ C}$) (Table S2) determined from DSC is

$$\text{R1306Q} < \text{I1309V} < \text{WT} < \text{G1324S}.$$

That is, R1306Q is the least stable; I1309V is slightly more stable, but still less stable than WT; and G1324S has the greatest stability. This rank order is reversed when comparing the bond lifetime at the lowest force measured:

$$\text{G1324S} < \text{WT} < \text{I1309V} < \text{R1306Q}.$$

At low force, the system is essentially under equilibrium (or near equilibrium), and the bond lifetime at low force is representative of the intrinsic stability of the A1-GPIbα bond. This inverse relationship between conformational stability and bond stability is shown in Fig. 7 *A*, where the bond lifetime at low force is plotted against the thermodynamic stability, ΔG^0, or $1/\Delta G^0$ (*inset* of Fig. 7 *A*), at 37°C. The data are inversely correlated and are well described by the empirical relationship in Eq. 1, where the *Constant* = 0.34 ± 0.04 (kcal s mol^{-1}) with a correlation coefficient $R = 0.983$,

$$\tau(s) = \frac{Constant}{\Delta G^0(\text{kcal/mol})}. \quad (1)$$

Therefore, a decrease in the native state stability of A1 relative to the intermediate resulting from the type 2B mutations will necessarily prolong low-force bond lifetime with GPIbα, whereas an increase in the native state stability of A1 will shorten low-force bond lifetime with GPIbα.

Comparing the mutational effects on the force required for maximal bond lifetime between A1 and GPIbα gives the

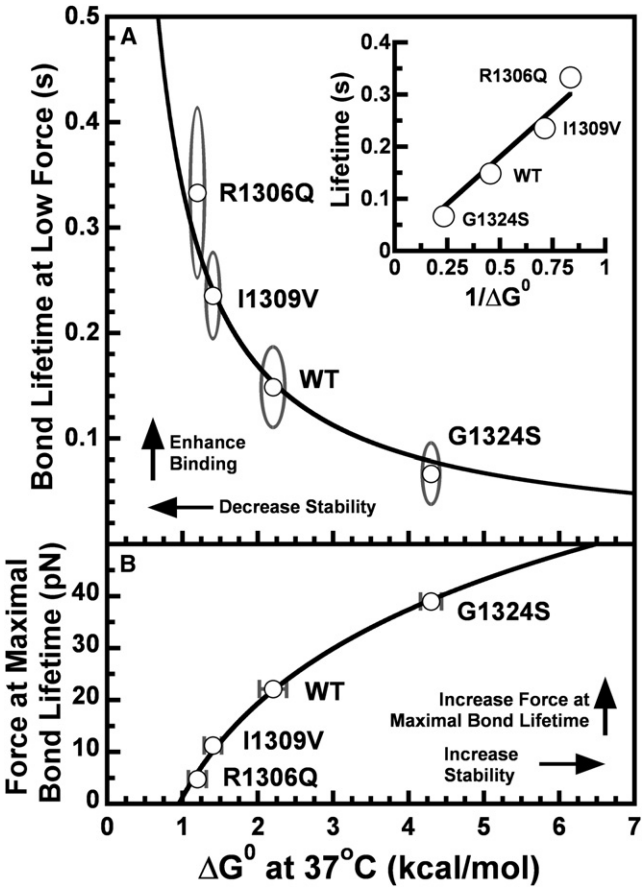

FIGURE 7 (*A*) Bond lifetime determined at low force (near equilibrium) for the interaction between A1 and GPIbα is inversely proportional to the thermodynamic stability of the A1 domain at 37°C. Shaded ellipses represent the error arcs for the experimental error on both the bond lifetime and ΔG^0. The fit to Eq. 1 was weighted according to the error on the lifetime measurements. (*Inset*) Linear plot of bond lifetime versus $1/\Delta G^0$. (*B*) Dependence of the force required for maximal bond lifetime on the thermodynamic stability of A1. As A1 stability increases, the force for maximal bond lifetime also increases.

same rank order as observed with conformational stability. That is, the force required for maximal bond lifetime, F_{max}, is lowest for R1306Q and greatest for G1324S. Fig. 7 *B* shows that increasing the conformational stability of A1 also increases the force at maximal bond lifetime. This force represents the transition from the catch to slip bonds shown in Fig. 6 and its dependence on conformational stability suggests that the force regulation of the A1-GPIbα dissociation is affected by the stability of A1. The most stable mutant, G1324S, requires the highest force to induce the transition from catch to slip bonds, whereas the least stable mutant, R1306Q, requires a force that is too low to be measured in our experiments.

DISCUSSION

The naturally occurring mutations in A1 domain of VWF examined in this study result in the phenotypes associated with types 2B (R1306Q, I1309V) and 2M (G1324S) VWD (29–31). Although all three of the mutations result in a hemorrhagic disorder, the type 2B is characterized by a gain-of-function phenotype in which the affinity of VWF for platelet GPIbα is enhanced, and therefore, platelet agglutination occurs at a lower concentration of the modulator ristocetin than normal plasma. Patients with the type 2M G1324S mutation, which results in a loss-of-function (defective binding to GPIbα) requires higher concentrations of ristocetin than normal to induce platelet agglutination (31). With these clinical observations in mind and the biophysical results described, there are several important points to be made to understand how these mutations alter the interaction between VWF and platelets.

Structural studies of the A1 domain with the type 2B mutations, R1306Q and I1309V, and A1 in complex with GPIbα, do not show significant conformational differences when compared to the WT structure (32–36). How then can the effects of these mutations be reconciled on a structural and conformational basis? We have approached this dilemma from a thermodynamic rationale and it is important to recognize that the thermodynamic studies are experiments conducted under equilibrium in solution. That is, the conformational stability of A1 determined at equilibrium represents an intrinsic property of the domain. We have found that the type 2B and 2M mutations have a significant effect on the intrinsic conformational stability of the A1 domain. At physiological temperature, type 2B mutations lower the stability and the type 2M mutation, G1324S, increases the stability of the A1 domain. Given the clinical observations of relative VWF-GPIbα affinity obtained from assays employing ristocetin, it is reasonable to hypothesize that a decreased conformational stability of A1 enhances its interaction with GPIbα, whereas an increase in A1 stability diminishes its interaction with GPIbα.

Because VWF functions under hydrodynamic forces that influence the structural stability of VWF, we have also studied the effect of the mutations on the dissociation kinetics of single A1-GPIbα bonds as a function of force by AFM. In these experiments, we observe a biphasic force-dependent pattern of bond lifetime in three of four cases, in which the bond lifetime increases with force to a maximum and then decreases with force. In fact, we previously related this catch-bond to slip-bond transition to the biphasic platelet rolling velocity on immobilized VWF as a function of shear stress (14). The effect of the mutations studied here is to shift this biphasic pattern either toward higher force (type 2M) or to lower force (type 2B).

The interpretation of these results is twofold.

First, the bond lifetime observed at low force is representative of the intrinsic propensity of A1 to bind GPIbα at equilibrium. In this regime, the bond lifetimes for the type 2B mutations are longer than observed for WT A1 and the type 2M mutation has a decreased bond lifetime relative to WT A1. Furthermore, the lifetimes of the A1-GPIbα

interaction are inversely proportional to the conformational stability of A1. This inverse correlation supports the hypothesis that a lower A1 stability enhances the affinity of VWF for platelets and a higher A1 stability decreases VWF-platelet affinity.

Second, the biphasic force dependence of the bond lifetimes is representative of the nonequilibrium effects of rheological shear. The peak of the force curves is the critical force required for the maximal bond lifetime for the A1-GPIbα interaction, and is directly correlated to the minimum of the biphasic platelet rolling-velocity curves as a function of shear rate that we recently described (14). This critical force, F_{max}, also has a functional dependence on the intrinsic conformational stability of A1. As the stability is increased, F_{max} also increases, and this implies that the greater the stability of A1, the greater the shear required for an optimal interaction between VWF and platelets. Therefore, the effects of VWD mutations on the intrinsic stability of A1 determine not only its equilibrium-binding propensity, but also the degree of rheological shear required for an optimal interaction with platelet GPIbα.

Since the binding propensity of A1 to GPIbα at equilibrium and under shear appears to be dependent on the intrinsic conformational stability of A1, the significance of the intermediate state is worth considering. At equilibrium, the unfolding of A1 proceeds through an intermediate state. The gain of function type 2B mutations decrease the stability of the native conformation of A1 and in doing so, shift the equilibrium in favor of this intermediate. At physiological temperature, the equilibrium population of the intermediate induced by the type 2B mutations is 10% or greater, which is significantly higher than WT A1 (~3%). Although it is not known whether the native to intermediate conformational transition of A1 occurs in full-length or multimeric VWF, our results support the idea that a VWF molecule containing a mutation that decreases the stability of the A1 structure could preferentially populate a conformation that exposes the GPIbα-binding site faster than WT VWF under low hydrodynamic forces. Therefore, it would spontaneously interact with platelets as described elsewhere (37). Within this context, it is possible that the intermediate state of A1 has a greater affinity for platelet GPIbα than the native state. In this case, the effect of shear forces on VWF may transiently shift the equilibrium in favor of the higher affinity intermediate conformation of A1 resulting in a decreased rate of dissociation and therefore an increased bond lifetime. The combined effect of shear and the destabilizing type 2B mutations investigated here may exacerbate this transient equilibrium resulting in a higher population of the intermediate in the presence of rheological stress. In contrast, we and others have demonstrated that the type 2M G1324S mutation in A1 impairs the conformational change required for the binding of VWF to GPIbα (15,37). This inhibitory effect of the G1324S mutation is likely a result of the increased structural stability of the A1 domain that inhibits the conformational transition from the native to intermediate state and restricts A1 to the low affinity native conformation.

The R1306Q mutation completely eliminates the catch-bond phase and has a structural stability lower than the I1309V mutation, which does not abolish the catch-bond phase but shifts the biphasic pattern to lower force. Interestingly, type 2B patients harboring either the R1306Q or the I1309V mutation or other mutations may present different clinical manifestations (38). For example, mild bleeding, normal platelet count, and lack of high molecular weight multimers of VWF have been described in patients containing the R1306Q mutation (39). Conversely, prolonged bleeding time, low platelet count (thrombocytopenia), spontaneous platelet aggregation, and some preservation of the high molecular weight multimers of VWF in plasma have been observed in patients with the I1309V mutation (30). In vivo, at high shear rates, it is possible that the VWF R1306Q mutant cannot bind firmly to platelet GPIbα, preventing platelet clearance from circulation and maintaining normal-to-moderate platelet counts. Previously, we described an interaction between the A1 and A2 domains (40) and it is possible that the effect of R1306Q on A1 stability may induce the neighboring A2 domain to effectively expose the cleavage site for ADAMTS-13, thereby reducing the larger multimers of VWF (41). On the other hand, at high shear rates, the VWF I1309V mutant may bind stably to platelets promoting spontaneous platelet agglutination, which depletes VWF from plasma and may cause thrombocytopenia. For the type 2M G1324S mutant, the VWF fails to interact with platelets because the mutation prevents the A1 domain from adopting a conformation that exposes the binding site for GPIbα. Therefore, bleeding results from depletion of larger VWF multimers from plasma, decreasing the platelet count and a defective VWF-GPIbα binding.

In summary, we have found that the type 2B and 2M mutations have a significant effect on the intrinsic conformational stability of the A1 domain. Changes in the conformational stability of A1 directly affect the force-dependent dissociation kinetics of VWF-GPIbα interactions. We have also demonstrated that platelet GPIbα can form catch bonds with type 2B VWF at low forces, which explains why thrombocytopenia can occur in type 2B von Willebrand Disease.

SUPPORTING MATERIAL

Two tables and six equations are available at http://www.biophysj.org/biophysj/supplemental/S0006-3495(09)00967-9.

We thank Dr. Jörg Rösgen for helpful discussions concerning the phase diagram method and Dr. Joel Moake for clinical insights and discussions on von Willebrand Disease. We also thank Dr. Pernilla Wittung-Stafshede for the use of her laboratory spectrometers and differential scanning calorimeter.

This work was supported by National Institutes of Health grant No. HL72886 (to M.A.C.) and grant No. HL091020 (to C.Z.), the Mary R. Gibson Foundation (to M.A.C. and M.A.), and the Baylor College of Medicine Thrombosis Research Training Grant (to M.A.).

REFERENCES

1. von Willebrand, E. 1926. Hereditary pseudohemophilia. *Finska Läkarsällskapetes Handl.* 68:87–112.
2. Federici, A. B., and P. M. Mannucci. 2007. Management of inherited von Willebrand disease in 2007. *Ann. Med.* 39:346–358.
3. Keeney, S., and A. M. Cumming. 2001. The molecular biology of von Willebrand disease. *Clin. Lab. Haematol.* 23:209–230.
4. Sadler, J. E. 1998. Biochemistry and genetics of von Willebrand factor. *Annu. Rev. Biochem.* 67:395–424.
5. Verweij, C. L., R. Quadt, E. Briet, K. Dubbeldam, G. B. Van Ommen, et al. 1988. Genetic linkage of two intragenic restriction fragment length polymorphisms with von Willebrand's disease type IIA. Evidence for a defect in the von Willebrand factor gene. *J. Clin. Invest.* 81:1116–1121.
6. Bonthron, D. T., R. I. Handin, R. J. Kaufman, L. C. Wasley, E. C. Orr, et al. 1986. Structure of pre-pro-von Willebrand factor and its expression in heterologous cells. *Nature.* 324:270–273.
7. Cruz, M. A., R. I. Handin, and R. J. Wise. 1993. The interaction of the von Willebrand factor-A1 domain with platelet glycoprotein Ib/IX. The role of glycosylation and disulfide bonding in a monomeric recombinant A1 domain protein. *J. Biol. Chem.* 268:21238–21245.
8. Cruz, M. A., T. G. Diacovo, J. Emsley, R. Liddington, and R. I. Handin. 2000. Mapping the glycoprotein Ib-binding site in the von Willebrand factor A1 domain. *J. Biol. Chem.* 275:19098–19105.
9. Sujimoto, M., J. Dent, R. McClintock, J. Ware, and Z. M. Ruggeri. 1993. Analysis of structure-function relationships in the platelet membrane glycoprotein Ib-binding domain of von Willebrand's factor by expression of deletion mutants. *J. Biol. Chem.* 268:12185–12192.
10. Miyata, S., and Z. M. Ruggeri. 1999. Distinct structural attributes regulating von Willebrand factor A1 domain interaction with platelet glycoprotein Ibα under flow. *J. Biol. Chem.* 274:6586–6593.
11. Favaloro, E. J. 2008. Phenotypic identification of platelet-type von Willebrand disease and its discrimination from type 2B von Willebrand disease: a question of 2B or not 2B? A story of nonidentical twins? Or two sides of a multidenominational or multifaceted primary-hemostasis coin? *Semin. Thromb. Hemost.* 34:113–127.
12. Meyer, D., E. Fressinaud, L. Hilbert, A.-S. Ribba, J.-M. Lavergne, et al. 2001. Type 2 von Willebrand disease causing defective von Willebrand factor-dependent platelet function. *Best Pract. Res. Clin. Haematol.* 14:349–364.
13. Auton, M., M. A. Cruz, and J. Moake. 2007. Conformational stability and domain unfolding of the von Willebrand factor A domains. *J. Mol. Biol.* 366:986–1000.
14. Yago, T., J. Lou, T. Wu, J. Yang, J. J. Miner, et al. 2008. Platelet glycoprotein Ibα forms catch bonds with human WT vWF but not with type 2B von Willebrand disease vWF. *J. Clin. Invest.* 118:3195–3207.
15. Morales, L. D., C. Martin, and M. A. Cruz. 2006. The interaction of von Willebrand factor-A1 domain with collagen: mutation G1324S (type 2M von Willebrand disease) impairs the conformational change in A1 domain induced by collagen. *J. Thromb. Haemost.* 4:417–425.
16. Romo, G. M., J. F. Dong, A. J. Schade, E. E. Gardiner, G. S. Kansas, et al. 1999. The glycoprotein Ib-IX-V complex is a platelet counterreceptor for P-selectin. *J. Exp. Med.* 190:803–814.
17. Lopez, M. M., and G. I. Makhatadze. 2002. Differential scanning calorimetry. *Methods Mol. Biol.* 173:113–119.
18. Hutter, J. L., and J. Bechhoefer. 1993. Calibration of atomic-force microscope tips. *Rev. Sci. Instrum.* 64:1868–1873.
19. Marshall, B. T., M. Long, J. W. Piper, T. Yago, R. P. McEver, et al. 2003. Direct observation of catch bonds involving cell-adhesion molecules. *Nature.* 423:190–193.
20. Sarangapani, K. K., T. Yago, A. G. Klopocki, M. B. Lawrence, C. B. Fieger, et al. 2004. Low force decelerates L-selectin dissociation from P-selectin glycoprotein ligand-1 and endoglycan. *J. Biol. Chem.* 279:2291–2298.
21. Ferreon, A. C., J. C. Ferreon, D. Bolen, and J. Rösgen. 2006. Protein phase diagrams II: non-ideal behavior of biochemical reactions in the presence of osmolytes. *Biophys. J.* 92:245–256.
22. Myers, J. K., C. N. Pace, and J. M. Scholtz. 1995. Denaturant *m*-values and heat capacity changes: relation to changes in accessible surface areas of protein unfolding. *Protein Sci.* 4:2138–2148.
23. Freire, E. 1994. Statistical thermodynamic analysis of differential scanning calorimetry data: structural deconvolution of heat capacity function of proteins. *Methods Enzymol.* 240:502–530.
24. Baskakov, I. V., and D. W. Bolen. 1999. The paradox between *m* values and δCp's for denaturation of ribonuclease T1 with disulfide bonds intact and broken. *Protein Sci.* 8:1314–1319.
25. Auton, M., L. M. Holthauzen, and D. W. Bolen. 2007. Anatomy of energetic changes accompanying urea-induced protein denaturation. *Proc. Natl. Acad. Sci. USA.* 104:15317–15322.
26. Lumry, R., and H. Eyring. 1954. Conformation changes of proteins. *J. Phys. Chem.* 58:110–120.
27. Plaza del Pino, I. M., B. Ibarra-Molero, and J. M. Sanchez-Ruiz. 2000. Lower kinetic limit to protein thermal stability: a proposal regarding protein stability in vivo and its relation with misfolding diseases. *Proteins.* 40:58–70.
28. Rodriguez-Larrea, D., B. Ibarra-Molero, L. de Maria, T. V. Borchert, and J. M. Sanchez-Ruiz. 2007. Beyond Lumry-Eyring: an unexpected pattern of operational reversibility/irreversibility in protein denaturation. *Proteins.* 70:19–24.
29. Hilbert, L., C. Gaucher, J. F. Abgrall, A. Parquet, C. Trzeciak, et al. 1998. Identification of new type 2B von Willebrand disease mutations: $Arg^{543}Gln$, $Arg^{545}Pro$ and $Arg^{578}Leu$. *Br. J. Haematol.* 103:877–884.
30. Federici, A. B., P. M. Mannucci, F. Stabile, M. T. Canciani, N. Di Rocco, et al. 1997. A type 2B von Willebrand disease mutation (Ile^{546}–>Val) associated with an unusual phenotype. *Thromb. Haemost.* 78:1132–1137.
31. Rabinowitz, I., E. A. Tuley, D. J. Mancuso, A. M. Randi, B. G. Firkin, et al. 1992. von Willebrand disease type B: a missense mutation selectively abolishes ristocetin-induced von Willebrand factor binding to platelet glycoprotein Ib. *Proc. Natl. Acad. Sci. USA.* 89:9846–9849.
32. Dumas, J. J., R. Kumar, T. McDonagh, F. Sullivan, M. L. Stahl, et al. 2004. Crystal structure of the wild-type von Willebrand factor A1-glycoprotein Ibα complex reveals conformation differences with a complex bearing von Willebrand disease mutations. *J. Biol. Chem.* 279:23327–23334.
33. Fukuda, K., T. A. Doggett, L. A. Bankston, M. A. Cruz, M. A. Diacovo, et al. 2002. Structural basis of von Willebrand factor activation by the snake toxin botrocetin. *Structure.* 10:943–950.
34. Huizinga, E. G., S. Tsuji, R. A. Romijn, M. E. Schiphorst, P. G. de Groot, et al. 2002. Structures of glycoprotein Ibα and its complex with von Willebrand factor A1 domain. *Science.* 297:1176–1179.
35. Emsley, J., M. Cruz, R. Handin, and R. Liddington. 1998. Crystal structure of the von Willebrand factor A1 domain and implications for the binding of platelet glycoprotein Ib. *J. Biol. Chem.* 273:10396–10401.
36. Celikel, R., K. I. Varughese, A. MadhusudanYoshioka, J. Ware, et al. 1998. Crystal structure of the von Willebrand factor A1 domain in complex with the function blocking NMC-4 Fab. *Nat. Struct. Biol.* 5:189–194.
37. Ajzenberg, N., A. S. Ribba, G. Rastegar-Lari, D. Meyer, and D. Baruch. 2000. Effect of recombinant von Willebrand factor reproducing type 2B or type 2M mutations on shear-induced platelet aggregation. *Blood.* 95:3796–3803.
38. Federici, A. B., P. M. Mannucci, G. Castaman, L. Baronciani, P. Bucciarelli, et al. 2008. Clinical and molecular predictors of thrombocytopenia and risk of bleeding in patients with von Willebrand disease type 2B: a cohort study of 67 patients. *Blood.* 113:526–534.
39. de Romeuf, C., L. Hilbert, and C. Mazurier. 1998. Platelet activation and aggregation induced by recombinant von Willebrand factors reproducing four type 2B von Willebrand disease missense mutations. *Thromb. Haemost.* 79:211–216.
40. Martin, C., L. D. Morales, and M. A. Cruz. 2007. Purified A2 domain of VWF binds to the active conformation of VWF and blocks the interaction with platelet GPIbα. *J. Thromb. Haemost.* 5:1363–1370.
41. Rayes, J., A. Hommais, P. Legendre, H. Tout, A. Veyradier, et al. 2007. Effect of von Willebrand disease type 2B and type 2M mutations on the susceptibility of von Willebrand factor to ADAMTS-13. *J. Thromb. Haemost.* 5:321–328.